

ProbeFlow: Training-Free Adaptive Flow Matching for Vision-Language-Action Models

Zhou Fang^{1,2}, Jiaqi Wang^{1,2}, Yi Zhou^{1,2*}, Qiongfeng Shi³

¹School of Computer Science and Engineering, Southeast University, China

²Key Laboratory of New Generation Artificial Intelligence Technology and Its Interdisciplinary Applications, Ministry of Education, China

³School of Electronic Science & Engineering, Southeast University, China

{220245032, 220242340, qiongfeng}@seu.edu.cn yizhou.szcn@gmail.com

Abstract—Recent Vision-Language-Action (VLA) models equipped with Flow Matching (FM) action heads achieve state-of-the-art performance in complex robot manipulation. However, the multi-step iterative ODE solving required by FM introduces inference latency that precludes responsive physical control. While current acceleration efforts optimize the Vision-Language Model (VLM) backbone, the action head bottleneck remains overlooked. To address this, we propose ProbeFlow, a training-free adaptive inference framework tailored for continuous robotic control. By evaluating geometric trajectory complexity via the cosine similarity between initial and lookahead velocity vectors, ProbeFlow dynamically schedules integration steps to prune redundant network evaluations. On the MetaWorld benchmark, it accelerates action decoding by $14.8\times$ (reducing average steps from $N = 50$ to 2.6) and cuts end-to-end system latency by $2.8\times$ without compromising the manipulation success rate. On the long-horizon LIBERO benchmark, the probe automatically allocates a denser schedule to navigate semantic bottlenecks, effectively resolving the flow solver delay. Real-world physical deployments confirm that ProbeFlow successfully mitigates action decoding latency while ensuring execution stability, offering a highly practical solution for low-latency continuous generative policies.

I. INTRODUCTION

Vision-Language-Action (VLA) models [1]–[3] demonstrate remarkable generalization by leveraging VLMs for reasoning. To translate perceptual representations into precise control, Flow Matching (FM) [4] has emerged as a promising action head. By modeling the behavior policy as a continuous-time probability flow, FM effectively captures complex, multi-modal action distributions and synthesizes high-precision manipulation trajectories with inherently straighter probability paths.

However, achieving low-latency real-time inference with Flow-based VLAs remains a formidable challenge. While current acceleration efforts predominantly optimize the Vision-Language Model (VLM) backbone [5]–[7], they overlook a fundamental architectural asymmetry in these continuous generative policies: while the vision-language backbone processes multimodal observations in a single forward pass, the FM action head requires multi-step iterative ODE solving. This necessitates repeatedly evaluating the heavy action

head network to decode a single action chunk. Consequently, standard fixed-step solvers (e.g., Euler with $N = 20$ steps) introduce a severe latency bottleneck, violating strict low-latency execution constraints. To address this bottleneck, we observe that generative probability paths in FM often exhibit distinct linear phases (e.g., gross transit motions) interspersed with highly curved regions (e.g., precise grasping). Relying on rigid, dense integration across the entire trajectory results in severe computational waste. Therefore, we propose **ProbeFlow**, an approach that dynamically aligns the computational cost with local trajectory complexity. By deploying a lightweight lookahead probe to foresee path curvature, it aggressively skips intermediate steps in linear regions, ensuring that dense integration is triggered only when strictly necessary.

In summary, our main contributions are as follows:

- We propose **ProbeFlow**, a training-free adaptive solver that mitigates the action decoding bottleneck in continuous generative policies, aligning them with strict low-latency constraints.
- We introduce a novel *Lookahead Linearity Probe*. By computing the cosine similarity between current and future velocity vectors as a geometric proxy for trajectory complexity, it strictly allocates network evaluations only in non-linear regions.
- Extensive evaluations on MetaWorld and LIBERO demonstrate that **ProbeFlow** fundamentally resolves the iterative decoding bottleneck. On MetaWorld, it accelerates the action head inference by $14.8\times$ while maintaining success rates. Real-world physical deployments further confirm its execution stability under real-time constraints.

An overview of the proposed framework is illustrated in Fig. 1.

II. RELATED WORK

A. Flow Matching in Vision-Language-Action Models

Flow Matching (FM) [4] has recently been adopted as a powerful action head for VLA models [2], [3] to model continuous-time probability flows. It effectively captures

*Corresponding author.

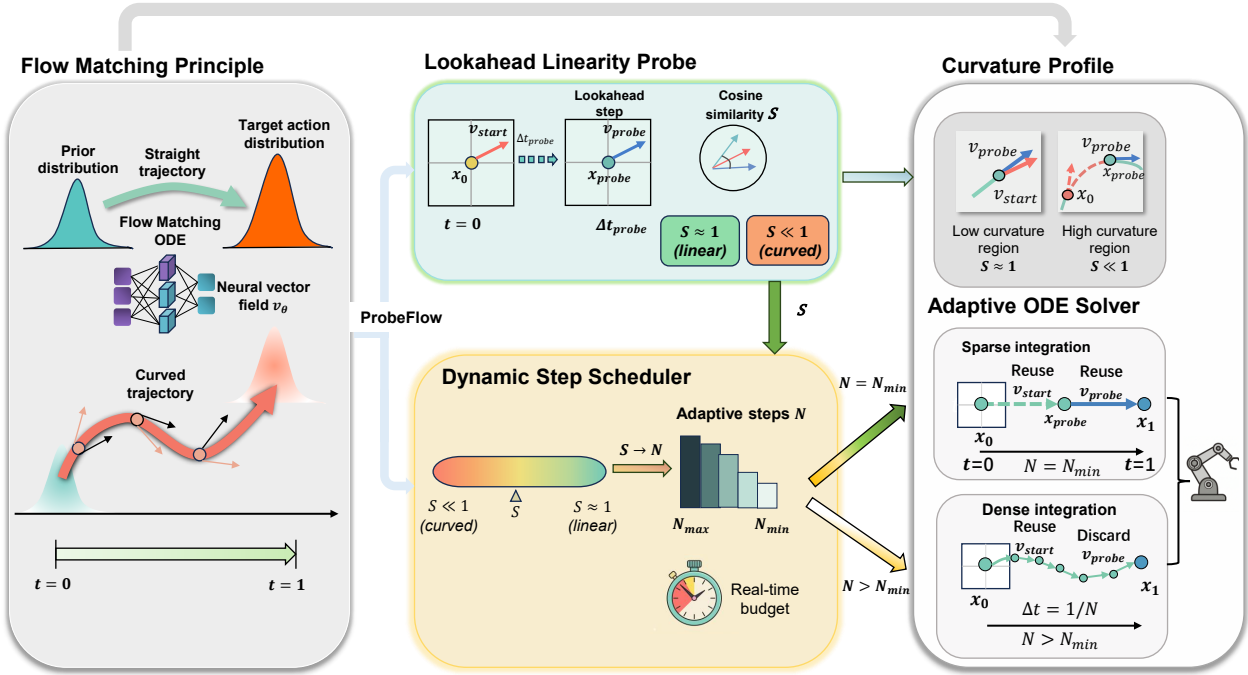


Fig. 1. Overview of the proposed **ProbeFlow** framework. **Left (Flow Matching Principle)**: Illustrates how generative probability paths exhibit varying degrees of curvature from prior to target action distributions. **Middle (Lookahead Linearity Probe & Dynamic Step Scheduler)**: The probe evaluates trajectory complexity via the cosine similarity \mathcal{S} between initial and lookahead velocities. The scheduler then dynamically maps \mathcal{S} to an adaptive step count N bounded by real-time budget constraints. **Right (Curvature Profile)**: In linear regions ($\mathcal{S} \approx 1$), it performs sparse integration by fully reusing probed states; in curved regions ($\mathcal{S} \ll 1$), it executes dense integration to bound truncation errors while still reusing the initial evaluation.

complex, multi-modal action distributions [8] and synthesizes highly precise manipulation trajectories [9], [10].

B. Efficiency Optimizations in VLA Models

To mitigate the heavy computational overhead of VLA models [11], current research predominantly focuses on optimizing the vision-language backbone via quantization [5] or token compression [6]. While these optimizations accelerate the perceptual forward pass, they overlook a critical bottleneck: the compute-intensive, iterative numerical integration within the generative action head.

To explicitly address the latency of action decoding, recent efforts have explored various acceleration strategies [11]. For continuous-time models, techniques such as consistency models [12] and rectified flow [13] have been proposed to compress the numerical integration steps. Concurrently, parallel and speculative decoding mechanisms are utilized to bypass discrete sequential token generation [14], [15]. Recent works have also explored adaptive computation; for instance, AdaFlow [16] dynamically adjusts integration steps for imitation learning by training an auxiliary variance estimation network. In a different vein, **ProbeFlow** approaches this from a purely geometric perspective, introducing a training-free probe that can be directly applied to pre-trained continuous generative policies without any additional optimization or parameter updates.

C. Advanced ODE Solvers in Generative Models

To accelerate continuous-time generative models, extensive efforts focus on optimizing numerical integration via advanced ODE/SDE solvers. These include high-order dedicated samplers like DPM-Solver [17], [18] and UniPC [19], as well as classical adaptive step-size algorithms like RK45 [20]. While these temporal solvers significantly reduce the Number of Function Evaluations (NFE) for high-fidelity offline generation, they pose inherent challenges for low-latency robotic closed-loop control. In contrast, **ProbeFlow** bypasses this multi-evaluation overhead via a single-shot lookahead probe, making it structurally aligned with the low-latency constraints of embodied AI.

III. PRELIMINARIES

A. Flow Matching for Action Generation

In the context of generative Vision-Language-Action (VLA) models, action generation can be formulated as learning a continuous-time probability path between a simple prior distribution and the complex, multi-modal distribution of expert demonstrations. Flow Matching (FM) provides a continuous-time framework to construct such paths by regressing a time-dependent vector field.

Let $x_0 \sim \mathcal{N}(0, \mathbf{I})$ be the initial noise state and $x_1 \sim q(x_1)$ be the ground-truth action chunk. FM constructs a probability density path $p_t(x)$ via linear interpolation $x_t = tx_1 + (1-t)x_0$, which naturally defines a constant target vector field

$\mathbf{u}_t(\mathbf{x}_t) = \mathbf{x}_1 - \mathbf{x}_0$. This transports the base distribution p_0 to the target distribution p_1 over continuous time $t \in [0, 1]$, governed by the ODE:

$$\frac{d\mathbf{x}_t}{dt} = \mathbf{u}_t(\mathbf{x}_t) = \mathbf{x}_1 - \mathbf{x}_0. \quad (1)$$

In practice, a neural network $\mathbf{v}_\theta(\mathbf{x}_t, t, \mathbf{c})$ is trained to approximate $\mathbf{u}_t(\mathbf{x}_t)$ using the following flow-matching regression objective:

$$\mathcal{L}(\theta) = \mathbb{E}_{t, \mathbf{x}_0, \mathbf{x}_1} [\|\mathbf{v}_\theta(\mathbf{x}_t, t, \mathbf{c}) - (\mathbf{x}_1 - \mathbf{x}_0)\|_2^2]. \quad (2)$$

Here, \mathbf{c} denotes the contextualized token embeddings output by the VLM backbone, which encode the raw visual observations and natural language instructions to condition the action generation.

B. Inference via Fixed-Step ODE Solvers

During deployment, generating an action trajectory requires solving the ODE parameterized by the trained network \mathbf{v}_θ . Since an exact analytical solution is generally unavailable, standard FM implementations rely on numerical integration. The most common solver in real-time robotics is the fixed-step Forward Euler method.

Given a predefined number of integration steps N , the time interval $[0, 1]$ is uniformly discretized into steps $\Delta t = 1/N$. Starting from pure noise \mathbf{x}_0 , the action state is iteratively updated as:

$$\mathbf{x}_{t+\Delta t} = \mathbf{x}_t + \Delta t \cdot \mathbf{v}_\theta(\mathbf{x}_t, t, \mathbf{c}). \quad (3)$$

While straightforward, the Forward Euler update effectively truncates second-order and higher terms. According to standard numerical analysis, this introduces a local truncation error e_{trunc} whose magnitude is strictly bounded by the temporal derivative of the velocity field (i.e., the trajectory curvature):

$$\|e_{\text{trunc}}\| \propto (\Delta t)^2 \left\| \frac{d\mathbf{v}_t}{dt} \right\|_2. \quad (4)$$

To maintain an acceptably low truncation error for physical robot execution, standard implementations typically require a small step size (e.g., $N \geq 50$). Consequently, the action head \mathbf{v}_θ must be evaluated N times sequentially to decode a single action chunk.

IV. METHODOLOGY

A. Inherent Geometric Linearity in Flow Matching

The fundamental premise of **ProbeFlow** stems from the explicit geometric objectives of Flow Matching (FM) and Rectified Flow [13]. Unlike traditional diffusion models that construct highly stochastic and heavily curved denoising trajectories [21], FM is mathematically formulated to construct deterministic ordinary differential equations (ODEs) with straight paths connecting the distributions. Specifically, it trains a neural vector field $\mathbf{v}_\theta(\mathbf{x}_t, t, \mathbf{c})$ to match the constant displacement vector $\mathbf{x}_1 - \mathbf{x}_0$ of the linear interpolation \mathbf{x}_t , effectively driving the prior distribution to the target action distribution along straight paths.

Theoretically, if the learned vector field perfectly achieves this objective, the velocity remains constant along each flow path ($\mathbf{v}_\theta(\mathbf{x}_t, t, \mathbf{c}) = \mathbf{x}_1 - \mathbf{x}_0$). Consequently, the entire ODE from $t = 0$ to $t = 1$ could be solved in an exact single Euler step without any truncation error.

However, in practical deployments, the action head $\mathbf{v}_\theta(\mathbf{x}_t, t, \mathbf{c})$ must approximate complex action distributions. Due to network capacity and non-linear task dynamics, the predicted vector field is rarely globally straight; instead, it exhibits varying curvature. This inherent geometric variation renders fixed-step solvers inefficient, presenting an opportunity to dynamically allocate computation only where the field is highly non-linear.

B. Lookahead Linearity Probe

To quantify the trajectory complexity, **ProbeFlow** introduces a highly efficient, one-shot *Lookahead Linearity Probe*. As established in Eq. (4), truncation error is governed by trajectory curvature. In highly linear phases (e.g., gross transit motions), the vector field is approximately constant ($\frac{d\mathbf{v}_t}{dt} \approx \mathbf{0}$). Here, truncation error structurally approaches zero, safely permitting large integration steps (e.g., $\Delta t \rightarrow 1$) without degrading action fidelity.

Rather than computing computationally prohibitive higher-order derivatives to estimate this curvature, our probe mechanism approximates this condition using discrete directional deviation.

Given the initial noise state \mathbf{x}_0 at integration time $t = 0$, we first compute the initial velocity vector using the trained flow matching action head:

$$\mathbf{v}_{\text{start}} = \mathbf{v}_\theta(\mathbf{x}_0, 0, \mathbf{c}). \quad (5)$$

Specifically, the probe executes a substantial exploratory step with a large interval Δt_{probe} (e.g., $\Delta t_{\text{probe}} = 0.5$) to project a future lookahead state:

$$\mathbf{x}_{\text{probe}} = \mathbf{x}_0 + \mathbf{v}_{\text{start}} \cdot \Delta t_{\text{probe}}. \quad (6)$$

Subsequently, we evaluate the vector field at this newly probed state:

$$\mathbf{v}_{\text{probe}} = \mathbf{v}_\theta(\mathbf{x}_{\text{probe}}, \Delta t_{\text{probe}}, \mathbf{c}). \quad (7)$$

To capture the directional deviation of the generative trajectory, we evaluate the cosine similarity between the initial and the lookahead velocity vectors as a geometric proxy for local curvature:

$$\mathcal{S} = \frac{\mathbf{v}_{\text{start}}^\top \mathbf{v}_{\text{probe}}}{\|\mathbf{v}_{\text{start}}\|_2 \|\mathbf{v}_{\text{probe}}\|_2}. \quad (8)$$

Geometrically, this similarity score represents the cosine of the angle θ between the initial projection direction and the actual local field at the probe location (i.e., $\mathcal{S} = \cos \theta$). As illustrated in Fig. 2, a similarity score $\mathcal{S} \approx 1$ ($\theta \approx 0^\circ$) signifies that the vector field is highly linear along the current path, safely allowing intermediate integration steps to be bypassed. Conversely, a lower score reveals that the linear probe has deviated from the true curved trajectory, creating a distinct angular deviation θ . This mathematically signals high local curvature and explicitly triggers the need for a denser integration schedule.

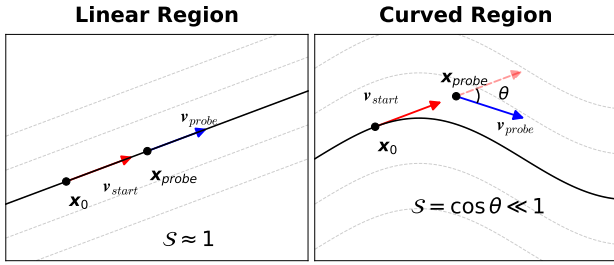


Fig. 2. Geometric principle of the Lookahead Linearity Probe in **ProbeFlow**. **Left (Linear Region)**: The linear probe step $\mathbf{x}_{\text{probe}}$ stays aligned with the true trajectory. The local field $\mathbf{v}_{\text{probe}}$ (blue) perfectly aligns with the initial velocity $\mathbf{v}_{\text{start}}$ (red), yielding high similarity ($S \approx 1$) and allowing aggressive step pruning. **Right (Curved Region)**: The linear probe overshoots the true curved trajectory. The resulting angular deviation θ between the ghost initial velocity (dashed red) and the actual local field (blue) causes a sharp drop in cosine similarity ($S = \cos \theta \ll 1$), correctly triggering a denser integration schedule to bound truncation errors.

C. Dynamic Step Scheduling and Integration

Once the trajectory linearity S is evaluated, **ProbeFlow** maps this continuous similarity score to a discrete number of integration steps N for the current control cycle. We formulate this adaptive allocation as a discrete scaling function:

$$N = \text{clip} \left(N_{\min} + \left\lfloor \frac{1-S}{\epsilon} \right\rfloor \times \Delta N, N_{\min}, N_{\max} \right), \quad (9)$$

where ϵ is a sensitivity hyperparameter defining the tolerance for directional deviation, ΔN denotes the discrete step increment size, and the bounds N_{\min} and N_{\max} explicitly constrain the computational budget to guarantee strict real-time execution frequencies.

Crucially, **ProbeFlow** minimizes computational overhead by formulating the state update as a conditional routing mechanism that maximizes state reuse. In highly linear regions ($N = N_{\min}$), the algorithm completely bypasses the intermediate integration and directly computes the final action state \mathbf{x}_1 :

$$\mathbf{x}_1 = \mathbf{x}_{\text{probe}} + \mathbf{v}_{\text{probe}} \cdot (1 - \Delta t_{\text{probe}}). \quad (10)$$

Here, the algorithm achieves negligible computational overhead by completely reusing both the initial evaluation $\mathbf{v}_{\text{start}}$ and the lookahead evaluation $\mathbf{v}_{\text{probe}}$. This absorbs the probing cost into the actual inference process. Conversely, in curved regions ($N > N_{\min}$), it computes the first intermediate state $\mathbf{x}_{\Delta t}$ to kickstart the denser integration schedule:

$$\mathbf{x}_{\Delta t} = \mathbf{x}_0 + \mathbf{v}_{\text{start}} \cdot \Delta t, \quad \text{where } \Delta t = 1/N. \quad (11)$$

While the lookahead evaluation $\mathbf{v}_{\text{probe}}$ is discarded in this scenario, the system still fully reuses the initial evaluation $\mathbf{v}_{\text{start}}$. This ensures that even when the vector field is highly curved, the extra cost of our linearity probe is at most one additional forward pass, preserving the overall real-time capability. The complete execution pipeline of our framework is summarized in Algorithm 1.

Algorithm 1 ProbeFlow Inference Pipeline

Require: Trained model \mathbf{v}_θ , Initial noise \mathbf{x}_0 , Condition \mathbf{c} , Threshold ϵ , Δt_{probe} , Bounds N_{\min}, N_{\max} , Increment ΔN

- 1: $\mathbf{v}_{\text{start}} \leftarrow \mathbf{v}_\theta(\mathbf{x}_0, 0, \mathbf{c})$
- 2: $\mathbf{x}_{\text{probe}} \leftarrow \mathbf{x}_0 + \mathbf{v}_{\text{start}} \cdot \Delta t_{\text{probe}}$
- 3: $\mathbf{v}_{\text{probe}} \leftarrow \mathbf{v}_\theta(\mathbf{x}_{\text{probe}}, \Delta t_{\text{probe}}, \mathbf{c})$
- 4: $S \leftarrow \frac{\mathbf{v}_{\text{start}}^\top \mathbf{v}_{\text{probe}}}{\|\mathbf{v}_{\text{start}}\|_2 \|\mathbf{v}_{\text{probe}}\|_2}$
- 5: $N \leftarrow \text{clip} \left(N_{\min} + \Delta N \times \left\lfloor \frac{1-S}{\epsilon} \right\rfloor, N_{\min}, N_{\max} \right)$
- 6: **if** $N = N_{\min}$ **then**
- 7: $\mathbf{x}_1 \leftarrow \mathbf{x}_{\text{probe}} + \mathbf{v}_{\text{probe}} \cdot (1 - \Delta t_{\text{probe}})$
- 8: **else**
- 9: $\Delta t \leftarrow 1.0/N$
- 10: $\mathbf{x}_t \leftarrow \mathbf{x}_0 + \mathbf{v}_{\text{start}} \cdot \Delta t$
- 11: $t \leftarrow \Delta t$
- 12: **for** $i = 1$ **to** $N - 1$ **do**
- 13: $\mathbf{v} \leftarrow \mathbf{v}_\theta(\mathbf{x}_t, t, \mathbf{c})$
- 14: $\mathbf{x}_t \leftarrow \mathbf{x}_t + \mathbf{v} \cdot \Delta t$
- 15: $t \leftarrow t + \Delta t$
- 16: **end for**
- 17: $\mathbf{x}_1 \leftarrow \mathbf{x}_t$
- 18: **end if**
- 19: **return** \mathbf{x}_1

V. EXPERIMENTS

In this section, we evaluate **ProbeFlow** to answer three key questions: **1) Efficiency & Effectiveness:** Can it substantially reduce inference latency without compromising manipulation success rates? **2) Dynamic Allocation:** Can the adaptive scheduler effectively distinguish between simple transit motions and complex bottlenecks to allocate steps proportionally? **3) Controllable Speed-Accuracy Trade-off:** Does the geometric threshold offer a predictable trade-off to adapt to different hardware constraints?

A. Experimental Setup

Model Architecture. We use the *Evo-I* [22] architecture with a frozen InternVL3-1B [23] visual backbone. The action head is a conditional Flow Matching network implemented via an 8-layer Diffusion Transformer (DiT [24]) with a 1024 hidden dimension, trained to predict trajectories of horizon $T = 50$.

Benchmarks. We evaluate on MetaWorld (MT50) [25] (50 short-horizon manipulation tasks) and LIBERO [26] (long-horizon, semantically complex tasks). For both, we report the average Success Rate (SR) and standard deviation over 10 evaluation episodes across 5 distinct random seeds.

Baselines & Implementation Details. We compare **ProbeFlow** against standard fixed-step Euler integration solvers with $N \in \{10, 20, 50\}$ steps. Furthermore, to evaluate high-order acceleration methods, we employ the classical second-order Adams-Bashforth (AB2 [27]) method. By reusing the velocity vector from the previous step, AB2 achieves second-order numerical accuracy without the heavy multi-evaluation overhead inherent in many advanced high-order solvers,

making it highly suitable for low-latency robotic control loops. We also include the classic adaptive-step RK45 solver as a baseline. Evaluation is performed on a single consumer-grade NVIDIA RTX 4090 GPU.

Crucially, to rigorously evaluate the training-free nature and task-agnostic generalization of **ProbeFlow**, no task-specific fine-tuning is applied. We formulate ϵ as a domain-level hyperparameter. For our main benchmark comparisons, we keep parameters strictly frozen across all tasks within a domain (setting $N_{\min} = 2, N_{\max} = 10, \Delta N = 2$, and $\epsilon = 0.008$ as the default across both MetaWorld and LIBERO to demonstrate baseline generalization).

B. Main Results: Latency Breakdown and Success Rate

To identify the computational bottleneck and evaluate our method, we profiled the end-to-end inference pipeline on the MetaWorld benchmark. As detailed in Table I, standard fixed-step solvers exhibit a severe trade-off between control latency and manipulation performance.

Using a standard 50-step Euler solver, the iterative Flow Matching head consumes **235.7 ms**, accounting for over 71% of the total inference latency. Because visual encoding imposes a fixed temporal overhead, this heavy ODE computation acts as the primary bottleneck restricting reactive control. While aggressively reducing the integration steps to 10 reduces the action head latency to 53.4 ms, it introduces substantial truncation error, causing a noticeable drop in the manipulation success rate.

Crucially, directly compressing the standard solver to an equivalent computational budget (Fixed-Euler $N = 3$) exposes the fragility of rigid integration, plunging the success rate to 72.4% due to fatal truncation errors at non-linear bottlenecks. In contrast, **ProbeFlow** effectively decouples the constant visual overhead by slashing the action head latency down to a mere **15.9 ms** (a **14.8 \times speedup** over the $N = 50$ solver) while maintaining an 83.2% success rate. This definitively confirms that our performance is a direct result of dynamic scheduling, rather than the flow model’s inherent robustness. Notably, **ProbeFlow** achieves a success rate ($83.2\% \pm 1.8\%$) strictly comparable to the $N = 50$ baseline ($82.5\% \pm 1.2\%$). The overlapping standard deviations indicate statistical parity. This confirms that our dynamic step scheduling safely prunes redundant network evaluations in linear regions without introducing harmful truncation errors. Rather than suffering from integration degradation, bypassing these intermediate steps avoids the computational waste of over-querying the imperfect neural vector field, thereby preserving the structural integrity of the generated trajectories.

Furthermore, our evaluation against advanced ODE solvers highlights the structural advantage of **ProbeFlow**. While the High-Order AB2 solver achieves second-order theoretical precision, its rigid step schedule yields an inferior 78.8% success rate. Similarly, the classic adaptive RK45 solver requires multiple internal network evaluations (typically 6 NFEs) per integration step to bound truncation errors. In the context of heavy VLA action heads, this internal NFE explosion

severely inflates the average inference latency to over 2900 ms, rendering it impractical for real-time robotic execution. In contrast, **ProbeFlow** measures trajectory curvature using a localized geometric proxy, costing at most one additional forward pass and minimal CPU-GPU synchronization overhead. This achieves a strictly superior Pareto boundary between decoding latency and manipulation fidelity, minimizing the algorithmic waste seen in traditional solvers.

C. Results on the LIBERO Benchmark

To rigorously evaluate the generalization of **ProbeFlow** in handling tasks with complex semantic visual observations and long-horizon dependencies, we extend our experiments to the LIBERO benchmark.

Unlike the short-horizon skills predominantly found in MetaWorld, LIBERO tasks involve multi-stage execution where the proportion of simple transit phases versus complex interaction phases varies significantly throughout a single episode. It is worth noting that the standard $N = 50$ baseline achieves a higher absolute success rate on LIBERO (92.5%) than on MetaWorld (82.5%). This discrepancy stems from the VLA model’s capacity bottleneck: MetaWorld’s 50 distinct kinematic tasks induce severe multi-task interference, capping the baseline, whereas LIBERO utilizes more homogeneous physical primitives but demands complex semantic reasoning. However, the true geometric complexity of the action flow is revealed by the numerical integration difficulty: preserving performance on LIBERO requires an average of 4.5 steps and still incurs a 3.8% relative performance drop, proving its probability paths are significantly more curved and challenging to solve than those in MetaWorld.

As shown in Table II, standard fixed-step solvers waste substantial computational budget across the long-horizon trajectory, with the $N = 50$ solver requiring 278.7 ms purely for action decoding. In contrast, **ProbeFlow** achieves an average of 4.5 steps, drastically compressing the flow solver latency to **32.7 ms** (an **8.5 \times speedup** over $N = 50$) while maintaining an 88.7% success rate. This action-head efficiency directly rivals the $N = 10$ baseline (89.0%, 54.5 ms) and vastly accelerates over the heavy $N = 20$ baseline (92.3%, 109.3 ms). By efficiently navigating the disparity between simple transit motions and complex interaction bottlenecks, **ProbeFlow** resolves the latency bottleneck. As detailed in Sec. V-E, tightening the threshold ($\epsilon = 0.002$) dynamically allocates more steps (average 14.1), recovering the success rate to 92.0% while remaining 60% faster than the $N = 50$ baseline.

D. Qualitative Analysis of Adaptive Scheduling

To understand the dynamic behavior of **ProbeFlow**, we visualized the step allocation across different manipulation phases, as illustrated in Fig. 3.

During simple spatial reaching or transit phases, where the optimal path is predominantly a straight line in the probability flow, the Lookahead Linearity Probe detects a high cosine similarity ($\mathcal{S} \approx 1.0$). This safely triggers the minimum step mode ($N = N_{\min}$), completely bypassing

TABLE I
INFERENCE LATENCY BREAKDOWN AND PERFORMANCE COMPARISON ON METAWORLD.

Method	Avg. Steps	Inference Latency (ms) ↓			Success Rate (%) ↑
		Visual Enc.	Flow Solver	Total	
Fixed-Euler ($N = 50$)	50.0	93.0	235.7	328.7	82.5 ± 1.2
Fixed-Euler ($N = 20$)	20.0	96.6	99.2	195.8	80.6 ± 0.6
Fixed-Euler ($N = 10$)	10.0	98.4	53.4	151.8	81.6 ± 1.3
Fixed-Euler ($N = 3$)	3.0	97.3	23.7	121.0	72.4 ± 1.2
RK45	68.9	100.3	2823.8	2924.1	63.0 ± 1.0
AB2	10.0	102.5	65.6	168.1	78.8 ± 0.8
ProbeFlow (Ours)	2.6	100.6	15.9	116.5	83.2 ± 1.8

TABLE II
INFERENCE LATENCY BREAKDOWN AND PERFORMANCE COMPARISON ON LIBERO.

Method	Avg. Steps	Inference Latency (ms) ↓			Success Rate (%) ↑
		Visual Enc.	Flow Solver	Total	
Fixed-Euler ($N = 50$)	50.0	107.6	278.7	386.3	92.5 ± 1.1
Fixed-Euler ($N = 20$)	20.0	111.1	109.3	220.3	92.3 ± 1.3
Fixed-Euler ($N = 10$)	10.0	106.9	54.5	161.4	89.0 ± 1.9
Fixed-Euler ($N = 5$)	5.0	104.7	34.0	138.7	86.9 ± 1.5
RK45	101.2	100.5	3769.3	3869.8	91.2 ± 1.1
AB2	10.0	117.2	66.9	184.0	88.9 ± 0.9
ProbeFlow (Ours)	4.5	106.4	32.7	139.1	88.7 ± 1.5

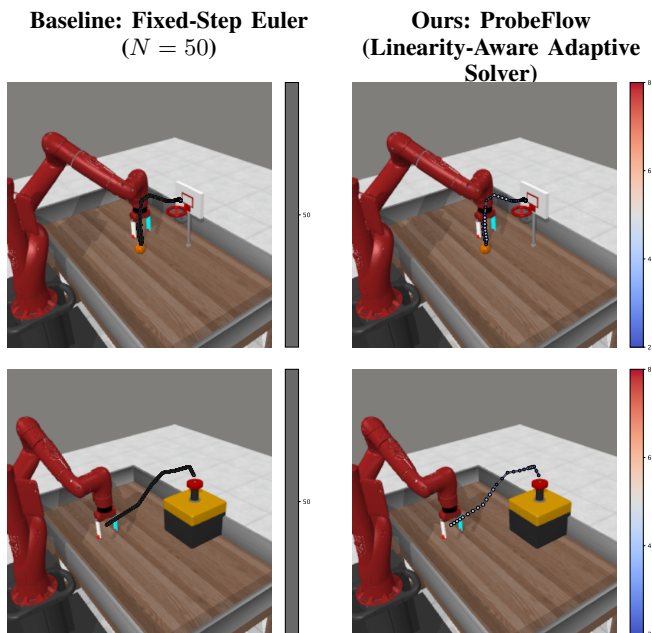


Fig. 3. Qualitative analysis of adaptive step scheduling. **Top:** In the complex Basketball task, **ProbeFlow** dynamically allocates denser steps (red) near critical interaction bottlenecks, such as object grasping and precise insertion. **Bottom:** In the Button Press task, it reliably assigns minimal steps (blue) during the linear transit phase.

intermediate network evaluations. Conversely, during complex phases such as precise object grasping, multi-stage interaction, or obstacle avoidance, the probe detects significant curvature in the vector field. It automatically scales up the step count to ensure fine-grained integration precision. This validates our core hypothesis: Flow Matching trajectories in robotic manipulation exhibit distinct linear phases that can

be aggressively exploited for efficient inference.

E. Robustness and Sensitivity Analysis

A critical requirement for deployment-ready robotic models is the avoidance of heavy re-training and per-task empirical tuning. We emphasize that the framework is strictly training-free. While N_{\min} and N_{\max} are determined by structural design and real-time hardware constraints, the sensitivity threshold ϵ is kept constant at the domain level. This reflects a deliberate trade-off between inference throughput and execution fidelity, rather than relying on task-specific parameter tuning.

Specifically, the maximum step bound N_{\max} is a strict upper limit dictated by the system’s real-time inference requirement (bounded to ensure the worst-case action decoding latency remains ≤ 200 ms). Conversely, $N_{\min} = 2$ represents the theoretical minimal integration steps required to utilize the initial and lookahead probe evaluations without computational waste.

Furthermore, the curvature threshold ϵ and step increment ΔN function merely as a coarse-grained quantization mechanism to map continuous linearity scores to discrete integration steps. To empirically validate this, we conducted a sensitivity analysis on a representative subset of MetaWorld tasks, as summarized in Table III.

By explicitly modulating the linearity tolerance $\epsilon \in \{0.001, 0.002, 0.004, 0.008\}$, we observe a highly predictable Pareto front. On the short-horizon MetaWorld benchmark (Table III), relaxing the threshold to $\epsilon = 0.008$ aggressively minimizes the action head latency (15.9 ms) while preserving the peak success rate (83.2%).

To further investigate this speed-accuracy trade-off on long-horizon, semantically complex tasks, we extend the sensitivity analysis to the LIBERO benchmark (Table IV).

TABLE III

SENSITIVITY ANALYSIS OF LINEARITY THRESHOLD ϵ ON METAWORLD.

Threshold ϵ	Avg. Steps	Action Head (ms) \downarrow	Success Rate (%)
$\epsilon = 0.001$	15.7	90.6	82.8 ± 0.3
$\epsilon = 0.002$	8.6	47.3	81.1 ± 2.0
$\epsilon = 0.004$	4.6	28.4	82.7 ± 1.3
$\epsilon = 0.008$	2.6	15.9	83.2 ± 1.8

TABLE IV

SENSITIVITY ANALYSIS OF LINEARITY THRESHOLD ϵ ON LIBERO.

Threshold ϵ	Avg. Steps	Action Head (ms) \downarrow	Success Rate (%)
$\epsilon = 0.001$	19.7	135.1	91.6 ± 1.2
$\epsilon = 0.002$	14.1	104.4	92.0 ± 1.0
$\epsilon = 0.004$	7.9	61.0	90.3 ± 0.8
$\epsilon = 0.008$	4.5	32.7	88.7 ± 1.5

Applying the aggressive $\epsilon = 0.008$ setting (optimal for MetaWorld) yields a highly efficient 4.5 steps, but intrinsically sacrifices execution precision (with the success rate dropping to 88.7%). However, tightening the threshold to $\epsilon = 0.002$ enables the scheduler to dynamically allocate an average of 14.1 steps. This effectively recovers the success rate to 92.0%, directly competitive with the heavy $N = 50$ baseline (92.5%), while still structurally reducing the action head latency by over 60%.

These results objectively demonstrate that a universally fixed threshold cannot perfectly harmonize the varying semantic complexities across different domains. Rather than a strictly zero-shot, cross-domain drop-in replacement, **ProbeFlow** functions as a highly controllable, training-free acceleration framework. By consciously calibrating the geometric tolerance ϵ , users can predictably navigate the fundamental trade-off between strict real-time latency constraints and the required manipulation fidelity for complex physical deployments.

Ablation on Lookahead Probe Horizon. The exploratory interval Δt_{probe} is the core structural parameter governing **ProbeFlow**'s phase-awareness. To validate its geometric rationale, we conducted a systematic ablation sweeping Δt_{probe} from 0.1 to 0.9, as depicted in Fig. 4.

The results reveal a stark performance dichotomy. When the probe horizon is excessively narrow ($\Delta t_{\text{probe}} \leq 0.4$), the probe acts myopically. It fails to detect impending vector field curvature, resulting in artificially high cosine similarity scores. Consequently, the scheduler erroneously forces the minimal step mode ($N \approx 2.0$), inducing massive truncation errors that precipitate a catastrophic collapse in success rate (below 5%). Conversely, when the probe steps too far into the future ($\Delta t_{\text{probe}} \geq 0.6$), it becomes over-sensitive. By directly comparing the initial state with drastically divergent distant states across non-linear boundaries, the similarity score drops precipitously. This triggers a conservative fallback, drastically inflating the average steps (surging to 20.0 at $\Delta t_{\text{probe}} = 0.9$). While it prevents the complete failure seen on the left side, it severely inflates the total inference latency to over 340 ms, completely nullifying the acceleration gains

Ablation on Lookahead Probe Horizon

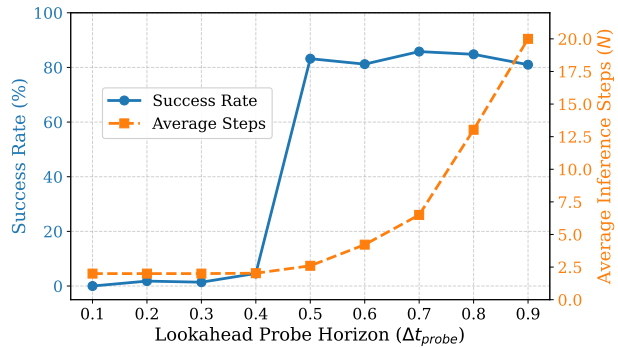


Fig. 4. Ablation study on the Lookahead Probe Horizon (Δt_{probe}) on MetaWorld. The dual-axis plot illustrates the critical trade-off between manipulation success rate (solid blue) and computational efficiency (dashed orange).

TABLE V

REAL-WORLD EVALUATION ON “PICK-AND-PLACE”

Method	Avg. Steps	Flow Solver (ms)	Success
Fixed-Euler ($N = 50$)	50.0	270.3	8/10
Fixed-Euler ($N = 20$)	20.0	99.9	7/10
Fixed-Euler ($N = 10$)	10.0	45.53	7/10
ProbeFlow (Ours)	2.1	12.26	7/10

of the framework.

The empirical sweet spot emerges sharply at $\Delta t_{\text{probe}} = 0.5$. By symmetrically bisecting the normalized ODE time-frames, it balances local linearity detection with global trajectory foresight, achieving a superior 83.2% success rate while requiring only 2.6 steps on average.

F. Real-World Deployment

To validate the physical execution capabilities and strict real-time viability of **ProbeFlow**, we deploy the framework in a real-world setting. The hardware setup consists of a 7-DoF UFACTORY xArm7 equipped with a 6-DoF Inspire multi-finger dexterous hand. Visual observations are captured via a fixed wrist-mounted Orbbec Gemini 360 camera, providing a consistent egocentric perspective for the VLA policy. The evaluation task is “Pick-and-Place”, which requires precise spatial tracking and reliable contact-rich grasping.

As shown in Fig. 5, the robot smoothly executes the contact-rich grasping of the apple and maintains precise trajectory tracking to place it onto the target plate. Quantitative results in Table V further demonstrate the practical superiority of our approach. Because the VLA model relies on high-resolution visual observations, our separated deployment architecture inherently suffers from substantial network communication latency. This physical transmission bottleneck imposes a heavy and relatively constant overhead per control cycle, making it the primary source of system delay and establishing a strict inherent lower bound for the end-to-end response time. By explicitly decoupling this dominant physical overhead from the computational cost, **ProbeFlow**

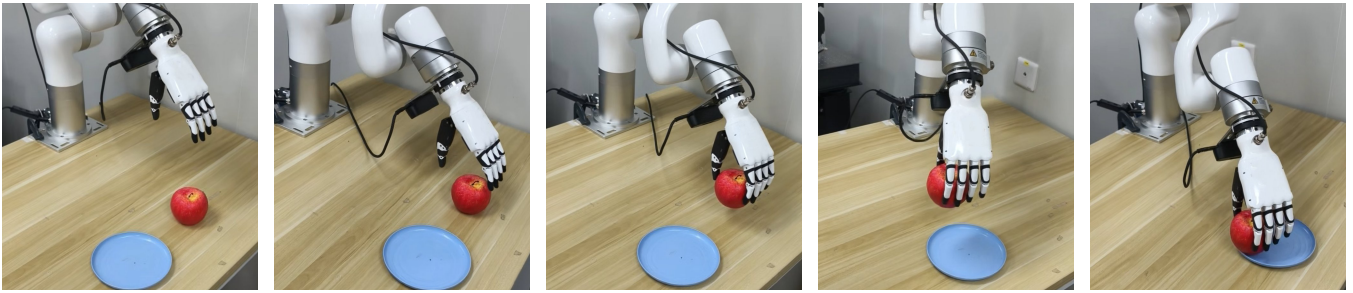


Fig. 5. Task progress of the real-world “Pick-and-Place” experiment. The sequence demonstrates **ProbeFlow** successfully executing continuous manipulation with a low-latency control loop.

directly targets the core algorithmic bottleneck on the action head. Compared to the computationally heavy $N = 50$ baseline, **ProbeFlow** significantly reduces the pure inference latency from 270.3 ms to a mere 12.26 ms, requiring only 2.1 steps on average. This structural acceleration ensures that the iterative generative policy execution does not exacerbate the unavoidable system-level network delay, providing a strictly bounded inference profile for real-world distributed robotic systems.

VI. CONCLUSION

We propose **ProbeFlow**, a training-free adaptive solver that resolves the iterative decoding bottleneck in Flow-Matching VLA models. Using a Lookahead Linearity Probe, it dynamically schedules ODE steps to prune redundant evaluations in linear paths. This drastically reduces latency while preserving manipulation fidelity in simulation and real-world deployments. While **ProbeFlow** is completely training-free, we acknowledge that optimal deployment across fundamentally different operational domains requires calibrating the linearity threshold. Furthermore, future work must validate this geometric scheduling against extreme non-linear dynamics in highly complex, contact-rich physical tasks, which extend beyond our proof-of-concept evaluation. Additionally, adapting the currently fixed lookahead horizon Δt_{probe} remains necessary to handle highly volatile trajectories.

REFERENCES

- [1] A. Brohan, N. Brown, J. Carbajal, Y. Chebotar, J. Dabis, C. Finn, K. Gopalakrishnan, K. Hausman, A. Herzog, J. Hsu *et al.*, “Rt-1: Robotics transformer for real-world control at scale,” *arXiv preprint arXiv:2212.06817*, 2022.
- [2] B. Zitkovich, T. Yu, S. Xu, P. Xu, T. Xiao, F. Xia, J. Wu, P. Wohlhart, S. Welker, A. Wahid *et al.*, “Rt-2: Vision-language-action models transfer web knowledge to robotic control,” in *Conference on Robot Learning*. PMLR, 2023, pp. 2165–2183.
- [3] M. J. Kim, K. Pertsch, S. Karamcheti, T. Xiao, A. Balakrishna, S. Nair, R. Rafailov, E. Foster, G. Lam, P. Sanketi *et al.*, “Openvla: An open-source vision-language-action model,” *arXiv preprint arXiv:2406.09246*, 2024.
- [4] Y. Lipman, R. T. Chen, H. Ben-Hamu, M. Nickel, and M. Le, “Flow matching for generative modeling,” *arXiv preprint arXiv:2210.02747*, 2022.
- [5] H. Wang, C. Xiong, R. Wang, and X. Chen, “Bitvla: 1-bit vision-language-action models for robotics manipulation,” *arXiv preprint arXiv:2506.07530*, 2025.
- [6] Y. Yang, Y. Wang, Z. Wen, L. Zhongwei, C. Zou, Z. Zhang, C. Wen, and L. Zhang, “Efficientvla: Training-free acceleration and compression for vision-language-action models,” *arXiv preprint arXiv:2506.10100*, 2025.
- [7] Y. Yue, Y. Wang, B. Kang, Y. Han, S. Wang, S. Song, J. Feng, and G. Huang, “Deer-vla: Dynamic inference of multimodal large language models for efficient robot execution,” *Advances in Neural Information Processing Systems*, vol. 37, pp. 56 619–56 643, 2024.
- [8] C. Chi, Z. Xu, S. Feng, E. Cousineau, Y. Du, B. Burchfiel, R. Tedrake, and S. Song, “Diffusion policy: Visuomotor policy learning via action diffusion,” *The International Journal of Robotics Research*, vol. 44, no. 10-11, pp. 1684–1704, 2025.
- [9] K. Black, N. Brown, D. Driess, A. Esmail, M. Equi, C. Finn, N. Fusai, L. Groom, K. Hausman, B. Ichter *et al.*, “ π_0 : A vision-language-action flow model for general robot control,” *arXiv preprint arXiv:2410.24164*, 2024.
- [10] J. Bjorck, F. Castañeda, N. Cherniadev, X. Da, R. Ding, L. Fan, Y. Fang, D. Fox, F. Hu, S. Huang *et al.*, “Gr00t n1: An open foundation model for generalist humanoid robots,” *arXiv preprint arXiv:2503.14734*, 2025.
- [11] Z. Yu, B. Wang, P. Zeng, H. Zhang, J. Zhang, L. Gao, J. Song, N. Sebe, and H. T. Shen, “A survey on efficient vision-language-action models,” *arXiv preprint arXiv:2510.24795*, 2025.
- [12] Y. Song, P. Dhariwal, M. Chen, and I. Sutskever, “Consistency models,” 2023.
- [13] X. Liu, C. Gong, and Q. Liu, “Flow straight and fast: Learning to generate and transfer data with rectified flow,” *arXiv preprint arXiv:2209.03003*, 2022.
- [14] W. Song, J. Chen, P. Ding, H. Zhao, W. Zhao, Z. Zhong, Z. Ge, J. Ma, and H. Li, “Accelerating vision-language-action model integrated with action chunking via parallel decoding,” *arXiv preprint arXiv:2503.02310*, 2025.
- [15] S. Wang, R. Yu, Z. Yuan, C. Yu, F. Gao, Y. Wang, and D. F. Wong, “Spec-vla: speculative decoding for vision-language-action models with relaxed acceptance,” in *Proceedings of the 2025 Conference on Empirical Methods in Natural Language Processing*, 2025, pp. 26 916–26 928.
- [16] X. Hu, Q. Liu, X. Liu, and B. Liu, “Adaflow: Imitation learning with variance-adaptive flow-based policies,” *Advances in Neural Information Processing Systems*, vol. 37, pp. 138 836–138 858, 2024.
- [17] C. Lu, Y. Zhou, F. Bao, J. Chen, C. Li, and J. Zhu, “Dpm-solver: A fast ode solver for diffusion probabilistic model sampling in around 10 steps,” *Advances in neural information processing systems*, vol. 35, pp. 5775–5787, 2022.
- [18] —, “Dpm-solver++: Fast solver for guided sampling of diffusion probabilistic models,” *Machine Intelligence Research*, vol. 22, no. 4, pp. 730–751, 2025.
- [19] W. Zhao, L. Bai, Y. Rao, J. Zhou, and J. Lu, “Unipc: A unified predictor-corrector framework for fast sampling of diffusion models,” *Advances in Neural Information Processing Systems*, vol. 36, pp. 49 842–49 869, 2023.
- [20] J. R. Dormand and P. J. Prince, “A family of embedded runge-kutta formulae,” *Journal of computational and applied mathematics*, vol. 6, no. 1, pp. 19–26, 1980.
- [21] J. Ho, A. Jain, and P. Abbeel, “Denosing diffusion probabilistic models,” *Advances in neural information processing systems*, vol. 33, pp. 6840–6851, 2020.
- [22] T. Lin, Y. Zhong, Y. Du, J. Zhang, J. Liu, Y. Chen, E. Gu, Z. Liu, H. Cai, Y. Zou *et al.*, “Evo-1: Lightweight vision-language-action model with preserved semantic alignment,” *arXiv preprint arXiv:2511.04555*, 2025.

- [23] J. Zhu, W. Wang, Z. Chen, Z. Liu, S. Ye, L. Gu, H. Tian, Y. Duan, W. Su, J. Shao *et al.*, “Internv13: Exploring advanced training and test-time recipes for open-source multimodal models,” *arXiv preprint arXiv:2504.10479*, 2025.
- [24] W. Peebles and S. Xie, “Scalable diffusion models with transformers,” in *Proceedings of the IEEE/CVF international conference on computer vision*, 2023, pp. 4195–4205.
- [25] T. Yu, D. Quillen, Z. He, R. Julian, K. Hausman, C. Finn, and S. Levine, “Meta-world: A benchmark and evaluation for multi-task and meta reinforcement learning,” in *Conference on robot learning*. PMLR, 2020, pp. 1094–1100.
- [26] B. Liu, Y. Zhu, C. Gao, Y. Feng, Q. Liu, Y. Zhu, and P. Stone, “Liber0: Benchmarking knowledge transfer for lifelong robot learning,” *Advances in Neural Information Processing Systems*, vol. 36, pp. 44 776–44 791, 2023.
- [27] K. Atkinson, W. Han, and D. E. Stewart, *Numerical solution of ordinary differential equations*. John Wiley & Sons, 2009.